Inorganic Chemistry

Article

pubs.acs.org/IC

Influence of the Steric Bulk and Solvent on the Photoreactivity of Ruthenium Polypyridyl Complexes Coordinated to L-Proline

Jordi-Amat Cuello-Garibo,[†] Elena Pérez-Gallent,[†] Lennard van der Boon,[†] Maxime A. Siegler,[‡] and Sylvestre Bonnet*[,†]

[†]Leiden Institute of Chemistry, Universiteit Leiden, Einsteinweg 55 2333 CC, Leiden, The Netherlands

[‡]Small Molecule X-ray Crystallography Facility, Johns Hopkins University, 3400 North Charles Street, Baltimore, Maryland 21218, United States

Supporting Information

ABSTRACT: Ruthenium polypyridyl complexes are good candidates for photoactivated chemotherapy (PACT) provided that they are stable in the dark but efficiently photosubstitute one of their ligands. Here the use of the natural amino acid L-proline as a protecting ligand for ruthenium-based PACT compounds is investigated in the series of complexes Λ-[Ru(bpy)$_2$(L-prol)]PF$_6$ ([**1a**]PF$_6$; bpy = 2,2′-bipyridine and L-prol = L-proline), Λ-[Ru(bpy)(dmbpy)(L-prol)]PF$_6$ ([**2a**]PF$_6$ and [**2b**]PF$_6$; dmbpy = 6,6′-dimethyl-2,2′-bipyridine), and Λ-[Ru(dmbpy)$_2$(L-prol)]PF$_6$ ([**3a**]PF$_6$). The synthesis of the tris-heteroleptic complex bearing the dissymmetric proline ligand yielded only two of the four possible regioisomers, called [**2a**]PF$_6$ and [**2b**]PF$_6$. Both isomers were isolated and characterized by a combination of spectroscopy and density functional theory calculations. The photoreactivity of all four complexes [**1a**]PF$_6$, [**2a**]PF$_6$, [**2b**]PF$_6$, and [**3a**]PF$_6$ was studied in water (H_2O) and acetonitrile (MeCN) using UV−vis spectroscopy, circular dichroism spectroscopy, mass spectrometry, and ^{1}H NMR spectroscopy. In H_2O, upon visible-light irradiation in the presence of oxygen, no photosubstitution took place, but the amine of complex [**1a**]PF$_6$ was photooxidized to an imine. Contrary to expectations, enhancing the steric strain by the addition of two ([**2b**]PF$_6$) or four ([**3a**]PF$_6$) methyl substituents did not lead, in phosphate-buffered saline (PBS), to ligand photosubstitution. However, it prevented photoxidation, probably as a consequence of the electron-donating effect of the methyl substituents. In addition, whereas [**2b**]PF$_6$ was photostable in PBS, [**2a**]PF$_6$ quantitatively isomerized to [**2b**]PF$_6$ upon light irradiation. In pure MeCN, [**2a**]PF$_6$ and [**3a**]PF$_6$ showed non-selective photosubstitution of both the L-proline and dmbpy ligands, whereas the non-strained complex [**1a**]PF$_6$ was photostable. Finally, in H_2O−MeCN mixtures, [**3a**]PF$_6$ showed selective photosubstitution of L-proline, thus demonstrating the active role played by the solvent on the photoreactivity of this series of complexes. The role of the solvent polarity and coordination properties on the photochemical properties of polypyridyl complexes is discussed.

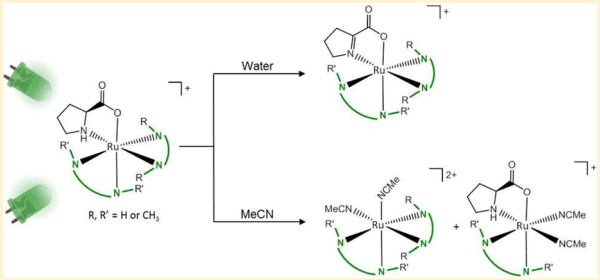

INTRODUCTION

Because of their unique photophysical and photochemical properties, ruthenium polypyridyl complexes have found many applications in supramolecular chemistry,[1−6] molecular imaging,[7−11] chemical biology,[12−14] and medicinal chemistry.[15] Notably, several groups are studying the biological activity of ruthenium-based photoactivated chemotherapy (PACT) prodrugs.[16−20] These compounds are non-toxic or poorly toxic in the dark, but they become highly cytotoxic, or more cytotoxic, upon visible-light irradiation. Unlike in photodynamic therapy, another phototherapeutic technique where phototoxicity comes from the light-induced generation of activated oxygen species such as singlet oxygen, in PACT light activation occurs via an oxygen-independent mechanism that often relies on ligand photosubstitution reactions.[21] Ligand photosubstitution in polypyridyl complexes is typically attributed to the thermal promotion of photogenerated triplet metal-to-ligand charge-transfer (^{3}MLCT) excited states into dissociative, low-lying triplet metal-centered (^{3}MC) excited states. In many reported examples, ruthenium PACT compounds are based on complexes of the [Ru(bpy)$_3$]$^{2+}$ family, where the photosubstituted ligand is a sterically hindered 2,2′-bipyridine (bpy) ligand such as 6,6′-dimethyl-2,2′-bipyridine (dmbpy).[19,22,23] The increased cytotoxicity is generally attributed to the intracellular formation of the *cis*-bis(aqua) complex [Ru(bpy)$_2$(OH$_2$)$_2$]$^{2+}$, which is believed to be the cytotoxic species. It should be noted, however, that the free dmbpy ligand is also generated upon light irradiation of [Ru(bpy)$_2$(dmbpy)]$^{2+}$, the biological properties and cytotoxicity of which have not been evaluated yet.

In order to specifically address the question of the cytotoxicity of the metal-containing fragment, we embarked on investigating whether natural amino acids such as L-proline

Received: November 21, 2016
Published: April 13, 2017

DOI: 10.1021/acs.inorgchem.6b02794
Inorg. Chem. 2017, 56, 4818−4828

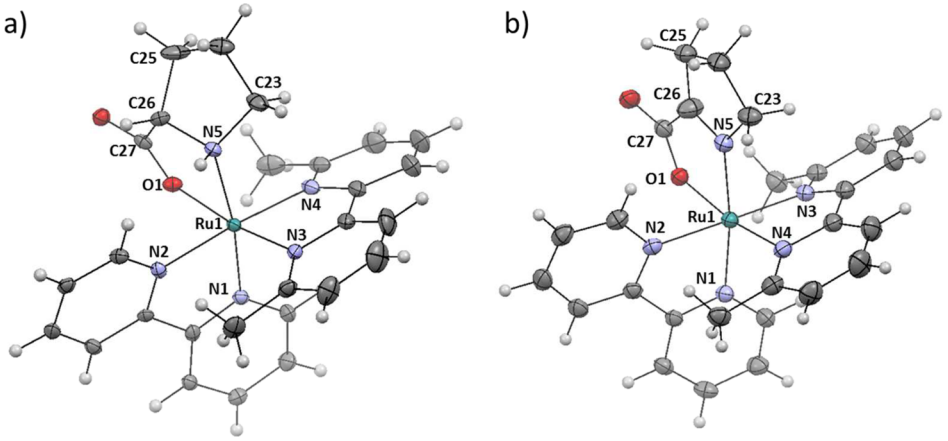

Figure 1. Crystal structures of (a) [**2b**]PF_6 and (b) [**2b**-2H]PF_6. Hexafluorophosphate counteranions, lattice H_2O, and disorder have been omitted for clarity.

Scheme 1. Structures of the Complexes [1a]PF_6, [2a]PF_6, [2b]PF_6, and [3a]PF_6

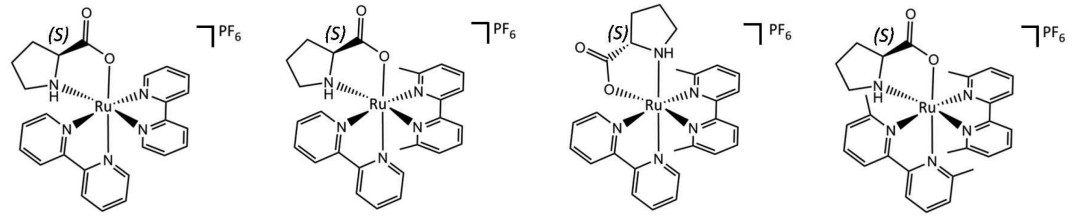

(L-prol), instead of hindered bipyridyl ligands, could be used to cage a *cis*-bis(aqua)ruthenium species. Amino acids are naturally present in a cell, so that the photochemical generation of 1 equiv of such ligands is not expected to have any impact on cell survival. For amino acid caged ruthenium polypyridyl complexes, any light-induced toxicity would be solely attributed to the metal fragment. In the literature, several examples of *cis*-ruthenium(II) diimine complexes coordinated to deprotonated L-amino acids were described that, upon light irradiation, interconvert between the Λ-L and Δ-L isomers.[24,25] However, to our knowledge, photosubstitution of an amino acid by solvent molecules has not been described yet. As reported for complexes with similar N,O-chelating ligands,[26−28] the strong σ-donor properties of the carboxylate moiety usually increase the e_g level of the metal complex and, therefore, the gap between the ^{3}MLCT and ^{3}MC states. Such an increased gap enhances the photostability of the complex by quenching photosubstitution reactions involving the ^{3}MC states. In order to recover ligand photosubstitution properties, sterically hindered chelates such as 6,6′-dmbpy can be reintroduced but, if possible, as spectator ligands to see whether the ^{3}MC states are low enough in energy to come in the vicinity of the photochemically generated ^{3}MLCT states.[29]

Of course, octahedral complexes bearing chiral and/or dissymmetric bidentate ligands such as amino acids can lead to the formation of many different isomers.[30] Thus, the preparation of such complexes is a priori challenging, although diastereoselective coordination reactions making use of interligand repulsion, and chromatographic separation techniques, have been described in the past.[31−33] Here, we report on the synthesis of a series of L-prol-bound ruthenium complexes comprising Λ-[Ru(bpy)$_2$(L-prol)]PF_6 ([**1a**]PF_6), Λ-[Ru(bpy)(dmbpy)(L-prol)]PF_6 ([**2a**]PF_6 and [**2b**]PF_6), and Λ-[Ru(dmbpy)$_2$(L-prol)]PF_6 ([**3a**]PF_6; Figure 1). In this series, the number of sterically hindering methyl groups increases from zero in [**1a**]PF_6 to two in [**2a**]PF_6 and [**2b**]PF_6) to four in [**3a**]PF_6. The influence of the solvent on the photoreactivity of these complexes was also investigated.

RESULTS AND DISCUSSION

Synthesis and Characterization. The four L-prol-coordinated ruthenium polypyridyl complexes were prepared as shown in Scheme 1. Complexes [**1a**]PF_6 and [**3a**]PF_6 were synthesized by reacting the C_2-symmetric precursor *rac*-[Ru(bpy)$_2$Cl$_2$] and *rac*-[Ru(dmbpy)$_2$Cl$_2$] ([**4**]), respectively, with L-prol.[34] As reported by Meggers et al., coordination of the chiral ligand L-prol to these racemic mixtures is diastereoselective and leads to the Λ-L diastereomer as a major ([**1a**]$^+$) or sole ([**3a**]$^+$) product.[34−36] The least hindered complex was obtained as a 17:1 [**1a**]$^+$/[**1b**]$^+$ mixture of diastereoisomers, where [**1b**]$^+$ is the Δ-L isomer. This mixture can further be resolved by silica column chromatography to obtain analytically pure samples of [**1a**]PF_6. On the other hand, the most hindered complex, [**3a**]PF_6, was directly obtained as a single Λ-L diastereoisomer without traces of the Δ-L diastereoisomer [**3b**]$^+$, as shown by the ^{1}H NMR of the crude product with a single set of 12 protons in the aromatic region (Figure S5).

The heteroleptic complexes [**2a**]PF_6 and [**2b**]PF_6 bear three different bidentate ligands and are less straightforward to prepare. Several methodologies to synthesize tris-heteroleptic ruthenium polypyridyl complexes are known in the literature, and most of them rely on the sequential addition of the different diimine ligands to a starting compound such as [Ru(CO)$_2$Cl$_2$]$_n$, *cis*-[Ru(DMSO)$_4$Cl$_2$] (DMSO = dimethyl sulfoxide), or [Ru(C$_6$H$_6$)Cl$_2$]$_2$.[37−42] However, for the synthesis of the tris-heteroleptic complex bearing one 6,6′-dmbpy,

DOI: 10.1021/acs.inorgchem.6b02794
Inorg. Chem. 2017, 56, 4818−4828

Scheme 2. Synthesis of [3a]PF_6, [2a]PF_6, and [2b]PF_6[a]

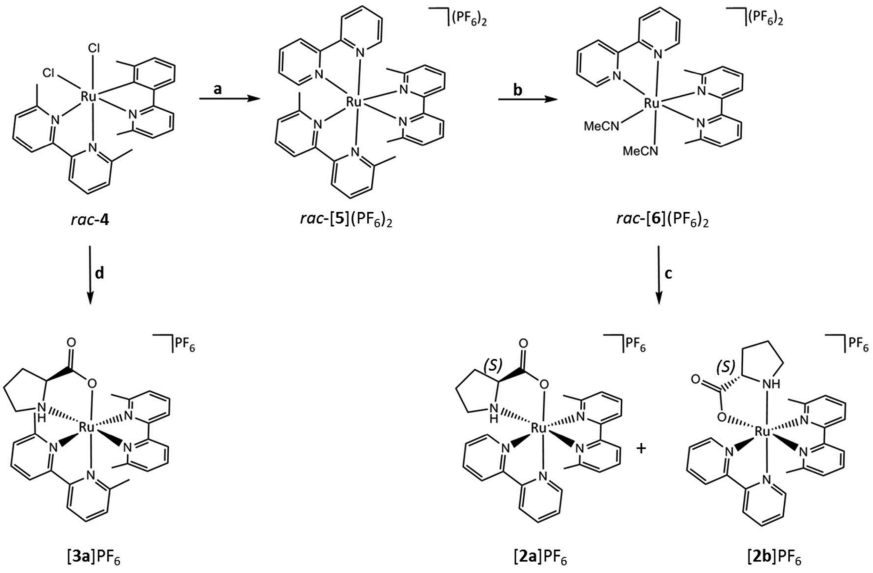

[a](a) (i) bpy (0.8 equiv), ethylene glycol, 3.5 h, 190 °C, pressure tube; (ii) KPF_6, 79%. (b) MeCN, 25 °C, white-light xenon lamp, 59%. (c) L-prol (2.5 equiv), K_2CO_3 (1.25 equiv), ethylene glycol, 40 min, 190 °C, pressure tube. (d) (i) L-prol (2.2 equiv), K_2CO_3 (1.1 equiv), ethylene glycol, 45 min, 190 °C, pressure tube; (ii) KPF_6, 56%.

[**2**]PF_6, we adapted a two-step synthesis introduced by von Zelewsky et al. using the highly strained $[Ru(bpy)(biq)_2]^{2+}$ species (where biq = 2,2′-biquinoline) as an intermediate, which, after irradiation in acetonitrile (MeCN), leads to the tris-heteroleptic precursor $[Ru(bpy)(biq)(MeCN)_2]^{2+}$.[43] With this method, we take advantage of the photoreactivity of strained ruthenium complexes and avoid the issues of adding 1 equiv of the first diimine ligand when other synthetic routes are used. Thus, as shown in Scheme 2, [**4**] was first converted into *rac*-$[Ru(bpy)(dmbpy)_2](PF_6)_2$ ([**5**]$(PF_6)_2$) by the addition of 1 equiv of bpy in ethylene glycol at 190 °C in a pressure tube. Limited ligand scrambling was observed, resulting in a sample containing also *rac*-$[Ru(dmbpy)_3](PF_6)_2$ and $[Ru(bpy)_2(dmbpy)](PF_6)_2$ as minor impurities [as observed by mass spectrometry (MS); Figure S7]. A solution of [**5**]$(PF_6)_2$ in MeCN was then irradiated using white light, whereby one dmbpy ligand was substituted by two solvent molecules to afford *rac*-$[Ru(bpy)(dmbpy)(MeCN)_2](PF_6)_2$ ([**6**]$(PF_6)_2$). Several impurities deriving from ligand scrambling and their photolysis products were present at that stage as well (Figure S8), but they could be removed for the most part after proline coordination. In the final step, L-prol was reacted with [**6**]$(PF_6)_2$ in ethylene glycol to yield the tris-heteroleptic complex [**2**]PF_6 in 62% yield as a mixture of isomers.

In octahedral complexes with two identical bpy or dmbpy ligands and one L-prol, the geometry is rather straightforward and only the two diastereoisomers Λ-L and Δ-L can exist. In contrast, for heteroleptic complexes with three different bidentate ligands, the geometry is more complex: besides the chirality of the octahedron (Λ or Δ) and that of the proline ligand (here only L), which generates two diastereoisomers, the two possible orientations of the N,O-dissymmetric proline ligand result in two different regioisomers. In other words, for the Λ-L and Δ-L isomers of [**2**]PF_6, either the amine group or the carboxylic acid moiety of proline is in the trans position to the dmbpy. The four possible diastereoisomers of $[\mathbf{2}]^+$ are named $[\mathbf{2a}]^+$, $[\mathbf{2b}]^+$, $[\mathbf{2c}]^+$, and $[\mathbf{2d}]^+$, and their structures are shown in Figure S26. According to ^{1}H NMR, the crude product [**2**]PF_6 was obtained, together with traces of [**3a**]PF_6, as a mixture of only two diastereoisomers in a ratio close to 1:1, as shown by the two characteristic doublets at 8.58 and 9.18 ppm corresponding to the position $H_{6'}$ on the bpy (Figure S2a). After purification by alumina chromatography using dichloromethane (DCM)/methanol (MeOH) (1−3%) as the eluent, this mixture could be resolved efficiently. The first fraction was obtained as an NMR-pure sample, whereas the second fraction was isolated as a mixture of a single isomer of [**2**]PF_6 and [**3a**]PF_6 in a ratio of 85:15 (Figures S2b,c, S3, and S4). Circular dichroism (CD) spectra of these two isomers in water (H_2O) showed a positive band at 300 nm for both isolated species (Figure S9), which means that they both have the Λ octahedral configuration.[44,45] As a consequence, these isomers are necessarily complexes [**2a**]PF_6 and [**2b**]PF_6 (Figure S26). NOESY analysis of [**2a**]PF_6 in deuterated water (D_2O) showed an off-diagonal correlation between the α proton of the L-prol ligand and the methyl substituent on the dmbpy, whereas no signal between those protons was found for complex [**2b**]PF_6 (Figure S6). In other words, the α proton and methyl substituent on the dmbpy are closer in complex [**2a**]PF_6 than in complex [**2b**]PF_6. Finally, single crystals suitable for X-ray structure determination were obtained for [**2b**]PF_6 by slow crystallization in H_2O. The space group (*P*1) was chiral, and the X-ray structure contained a single configuration of the coordination octahedron (Λ). The molecular structure, shown in Figure 1a, showed a long N5−C26 single bond [1.510(5) Å] for the proline ligand, and the oxygen atom of L-prol was found trans to the dmbpy ligand (Table 1). Thus, the nature of the isomer [**2b**]PF_6 was unequivocally confirmed, and as a consequence, [**2a**]PF_6 was analyzed as the Λ-L isomer having the oxygen atom trans to the bpy ligand.

Density functional theory (DFT) calculations of both diastereoisomers Λ-L and Δ-L of $[\mathbf{1}]^+$ and $[\mathbf{3}]^+$, and the four possible diastereoisomers of $[\mathbf{2}]^+$, were performed in H_2O using the conductor-like screening model (COSMO) to simulate solvent effects (see the Supporting Information). The optimized structures, their energies in H_2O, and their

DOI: 10.1021/acs.inorgchem.6b02794
Inorg. Chem. 2017, 56, 4818−4828

Table 1. Selected Bond Lengths (Å) and Angles (deg) for [2b]PF_6 and [2b-2H]PF_6

	[2b]PF_6	[2b-2H]PF_6
Ru1−O1	2.100(3)	2.111(1)
Ru1−N1	2.024(3)	2.047(1)
Ru1−N2	2.067(4)	2.066(2)
Ru1−N3	2.074(3)	2.074(2)
Ru1−N4	2.098(4)	2.067(2)
Ru1−N5	2.143(3)	2.046(1)
N5−C26	1.510(5)	1.305(3)
C25−C26−N5	115.5(2)	106.0(3)
C23−N5−C26−C27	122.1(4)	−174.4(2)

dipole moments are given in Figure S26 and Table S4, respectively. In H_2O, the Λ complexes [**1a**]$^+$ and [**3a**]$^+$ are 6.9 and 19.6 kJ·mol^{-1} more stable than their Δ diastereoisomers [**1b**]$^+$ and [**3b**]$^+$, respectively. These results confirmed that the diastereoselectivity of L-prol coordination to [Ru(bpy)$_2$Cl$_2$] or [Ru(dmbpy)$_2$Cl$_2$] is enhanced when hindering methyl substituents are put on the bpy ligands. For the heteroleptic complex [**2**]$^+$, of all four isomers, the isomer [**2b**]$^+$ was found to be the most stable in H_2O, followed by [**2a**]$^+$, [**2d**]$^+$, and [**2c**]$^+$, at +1.9 kJ·mol^{-1}, +2.2 kJ·mol^{-1}, and +25.7 kJ·mol^{-1}, respectively. Although [**2c**]$^+$ clearly is too high in energy to be formed under thermodynamic control, its isomers [**2a**]$^+$, [**2b**]$^+$, and [**2d**]$^+$ are too close in energy to predict any stereoselectivity based on thermodynamic arguments. The fact that [**2d**]$^+$ is not observed experimentally can be interpreted as a sign that the coordination of L-prol to [Ru(bpy)(dmbpy)(MeCN)$_2$]$^{2+}$ is under kinetic control. DFT models could also be used to find signs of steric hindrance in this series of complexes. The structural distortion parameters, i.e., the bond angle variance (σ^2) and the mean quadratic elongation (λ), were calculated for complexes [**1a**]$^+$, [**2b**]$^+$, and [**3a**]$^+$ (Table S5).[46−48] The values found, 50.5, 75.7, and 90.4 (σ^2) and 2.21 × 10^{-4}, 2.50 × 10^{-4}, and 3.06 × 10^{-4} (λ), respectively, confirmed that the addition of two or four methyl substituents at the 6 and 6′ positions of the bpy ligands has a major impact on the distortion of the octahedral sphere of the ruthenium complexes. Surprisingly, this distortion has no significant effect on the Ru−O bond distances, being 2.109, 2.105, and 2.109 Å in complexes [**1a**]$^+$, [**2b**]$^+$, and [**3a**]$^+$ respectively.

Photochemistry. The photoreactivity of [**1a**]PF_6 was studied first. The evolution of the UV−vis spectrum of a solution of [**1a**]PF_6 in phosphate-buffered saline (PBS) was studied upon irradiation at 493 nm under air. An hypsochromic shift in the ^{1}MLCT band was observed, with a change in the absorption maximum from 495 to 467 nm and an isosbestic point at 486 nm (Figure 2a). Furthermore, the MS spectrum after irradiation showed a peak at m/z 526.1 (Figure 3a), which is two units smaller than the starting complex (calcd m/z 528.1). These two units correspond to the loss of two hydrogen atoms. According to Keene et al., these hydrogen atoms may correspond to the α-hydrogen and amine hydrogen of proline, i.e., the imine complex [Ru(bpy)$_2$(L-prol-2H)]PF_6 ([**7**]PF_6) was formed.[49] A quantum yield (φ_{PS}) of 0.0010 was calculated for this photoreaction in PBS (Figure S14); and a dark control experiment at 37 °C did not show any change in the UV−vis spectrum over time (Figure S11), which excludes a thermal reaction under light irradiation. The oxidative nature of the photoreaction was confirmed by performing the same photoreaction under argon. No change in either the UV−vis (Figure 2b) or MS (Figure 3c) spectrum was observed in the absence of oxygen. When following the irradiation by NMR under argon, a new doublet appeared at 8.91 ppm, which corresponds to the Δ-L isomer [**1b**]$^+$ (Figure S10).[34] In addition, a decrease in the band at 300 nm in the CD spectra was observed upon irradiation under the same conditions (Figure S13). Finally, the addition of the antioxidant glutathione (GSH) before

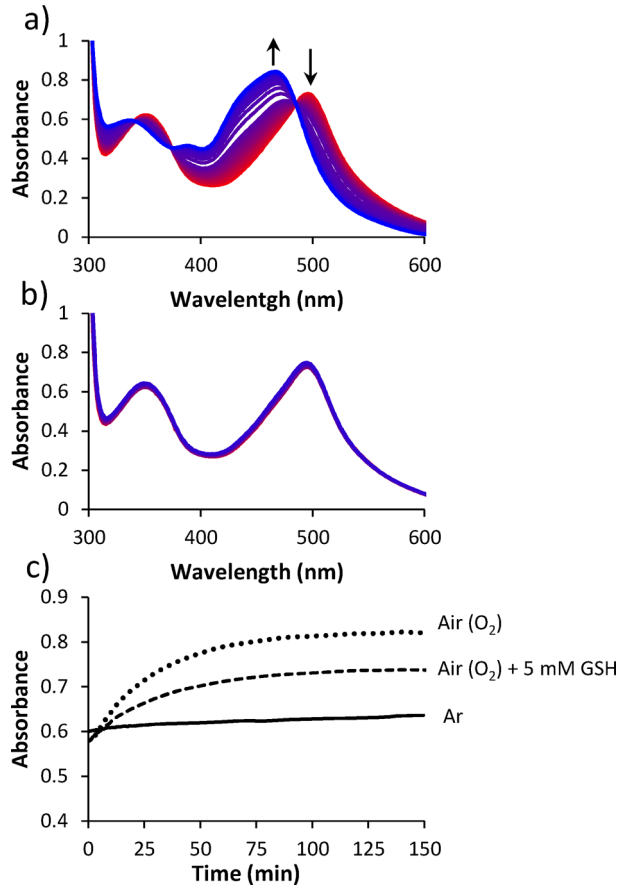

Figure 2. Evolution of the UV−vis spectra of a 0.078 mM solution of [**1a**]PF_6 in PBS irradiated at 298 K with a 493 nm LED at 12.0 mW·cm^{-2} (a) under air and (b) under argon. (c) Evolution of the absorbance at 473 nm upon irradiation under air (dotted line), under air in the presence of 5 mM GSH (dashed line), and under argon (solid line).

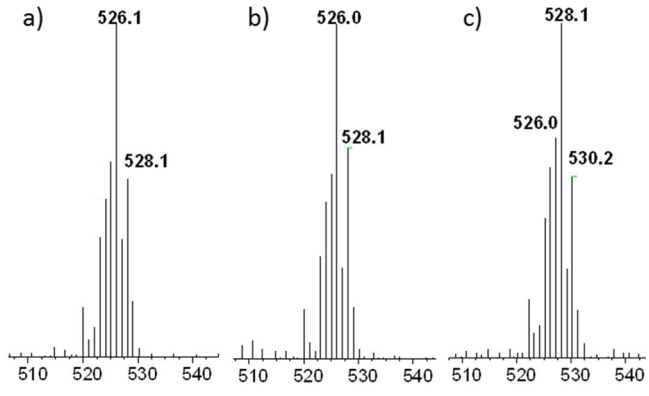

Figure 3. MS spectrum of a 0.078 mM solution of [**1a**]PF_6 in PBS after light irradiation at 298 K with a 493 nm LED at 12.0 mW·cm^{-2} (a) under air, (b), under air in the presence of 5 mM GSH, and (c) under argon. The conditions are detailed in Table S2.

DOI: 10.1021/acs.inorgchem.6b02794
Inorg. Chem. 2017, 56, 4818−4828

irradiation in air partially slowed down the photoreaction (Figures 2c and S12a). In such conditions, MS after 180 min of irradiation (Figure 3b) showed a mixture of $[\mathbf{1a}]^+$ (m/z 528.1) and $[7]^+$ (m/z 526.1) because the relative intensity of the m/z 528.1 peak in the isotopic pattern of $[7]PF_6$ was slightly higher than expected, as shown in the calculated isotopic pattern for a given mixture of 7:3 $[\mathbf{1}]^+/[7]^+$ in Figure S15. In order to confirm that irradiation led to photooxidation and compare our results under light irradiation to that obtained using electrochemical oxidation by Yamaguchi et al.,[50] a spectroelectrochemistry analysis of $[\mathbf{1a}]PF_6$ was performed. Chronoamperometry of a solution of $[\mathbf{1a}]PF_6$ in PBS with a constant potential of +0.645 V vs Ag/AgCl using carbon sponges as working and counter electrodes was followed by UV−vis spectroscopy. After 2 h, the current stabilized at 0.05 mA, and the oxidative reaction was considered to be finished. As shown in Figures S23b and S25, the UV−vis and MS spectra showed the same changes as those upon light irradiation, i.e., a hypsochromic shift from 495 to 466 nm in the MLCT band with an isosbestic point at 486 nm and a peak at a m/z 526.1. Thus, as shown in Scheme 3, upon light irradiation of $[\mathbf{1a}]^+$ under argon, partial photoisomerization from Λ-L to Δ-L takes place, as has been described extensively in the literature for *cis*-ruthenium(II) diimine complexes coordinated to a deprotonated amino acid.[24,25] However, in the presence of dioxygen, the coordinated ligand L-prol is oxidized to its imino analogue $[7]^+$, as described for the complex $[Ru(bpy)_2(2\text{-}(1\text{-aminoethyl})(pyridine)](PF_6)_2$ by Keene et al. or for $[Os(bpy)_2(2\text{-aminoehanesulfinate})](PF_6)$ by Tamura et al.[49,51] Although the exact mechanism of photooxidation is unclear, we suggest that the amine may be oxidized by the singlet oxygen ($^1O_2$) generated in the presence of light and molecular oxygen because it has been demonstrated that $^1O_2$ is a much better oxidant than the ground state $^3O_2$.[52] More in-depth studies would be needed to confirm this hypothesis.

Scheme 3. Scheme of the Photoisomerization and Photoxidation Observed upon Visible-Light Irradiation of $[\mathbf{1a}]PF_6$ in PBS at 298 K with a 493 nm LED at 12.0 mW·cm^{-2}

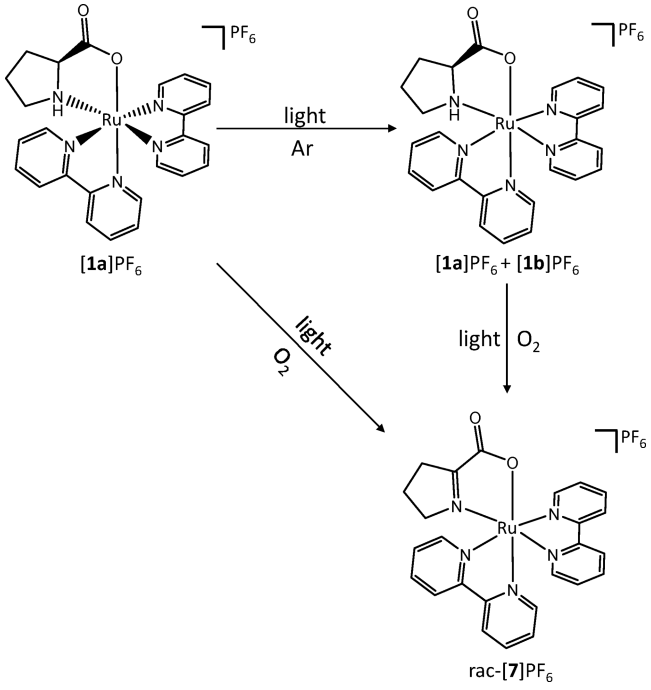

In a second step, the reactivity of the more hindered complexes, $[\mathbf{2a}]PF_6$, $[\mathbf{2b}]PF_6$, and $[\mathbf{3a}]PF_6$, was investigated. When a solution of $[\mathbf{3a}]PF_6$ was irradiated in PBS at 493 nm under air, no change in the UV−vis or MS spectra was observed (Figures 4a and S12d). Like for $[\mathbf{1a}]^+$, partial isomerization from Λ-L to Δ-L occurred as shown by the decrease of the band at 300 nm in the CD spectrum (Figure S17). Thus, for complex $[\mathbf{3a}]PF_6$, photooxidation did not occur in PBS, which represents a dramatic change compared to the photoreactivity of $[\mathbf{1a}]PF_6$. Suprisingly, the much higher steric hindrance of the complex did not lead to photosubstitution reactions either. On the other hand, when a solution of $[\mathbf{2a}]PF_6$ in PBS was irradiated with a 1000 xenon lamp equipped with a 450 nm blue-light filter and followed by ^1H NMR, a doublet at 9.1 ppm, characteristic of the 6′ proton of the bpy ligand in $[\mathbf{2b}]PF_6$, arose upon 15 min irradiation. In such conditions, photoconversion of $[\mathbf{2a}]PF_6$ to $[\mathbf{2b}]PF_6$ was complete after 150 min

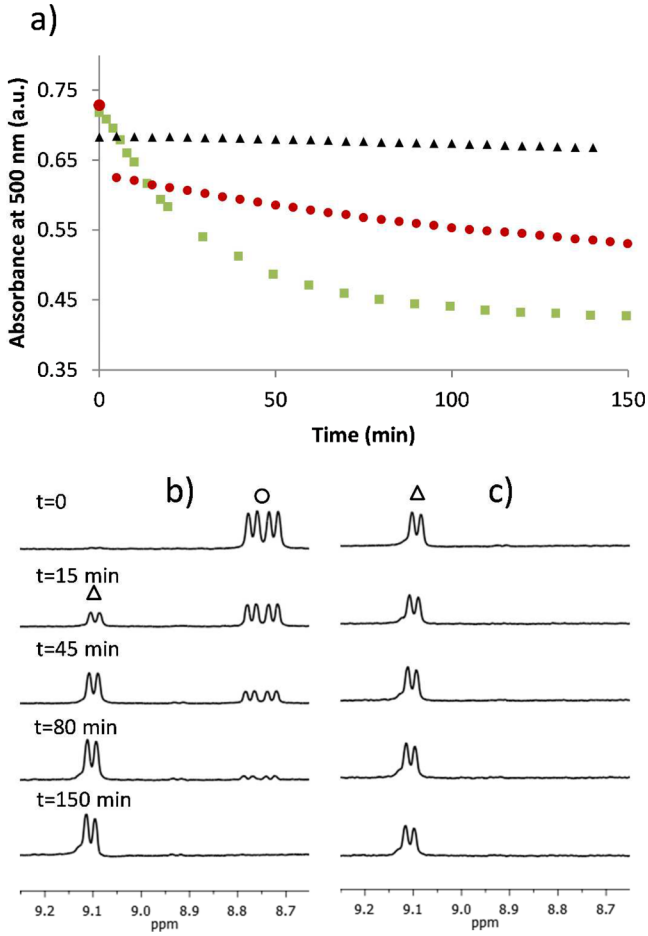

Figure 4. (a) Evolution of the absorption at 500 nm of a solution of $[\mathbf{1a}]PF_6$ (0.078 mM, red circles), $[\mathbf{2a}]PF_6$ (0.032 mM, green squares), and $[\mathbf{3a}]PF_6$ (0.077 mM, black triangles) in PBS upon irradiation under air with a 493 nm LED at 12.0, 8.7, and 11.0 mW·cm^{-2}, respectively. The conditions are detailed in Table S2. (b) Evolution of the ^1H NMR of a D_2O solution of (b) $[\mathbf{2a}]PF_6$ (2.7 mg in 0.7 mL, circles) and (c) $[\mathbf{2b}]PF_6$ (2.6 mg in 0.7 mL, triangles) upon light irradiation with the beam of a xenon lamp filtered with a 450 nm blue-light filter under air. The conditions are detailed in the Supporting Information.

DOI: 10.1021/acs.inorgchem.6b02794
Inorg. Chem. 2017, 56, 4818−4828

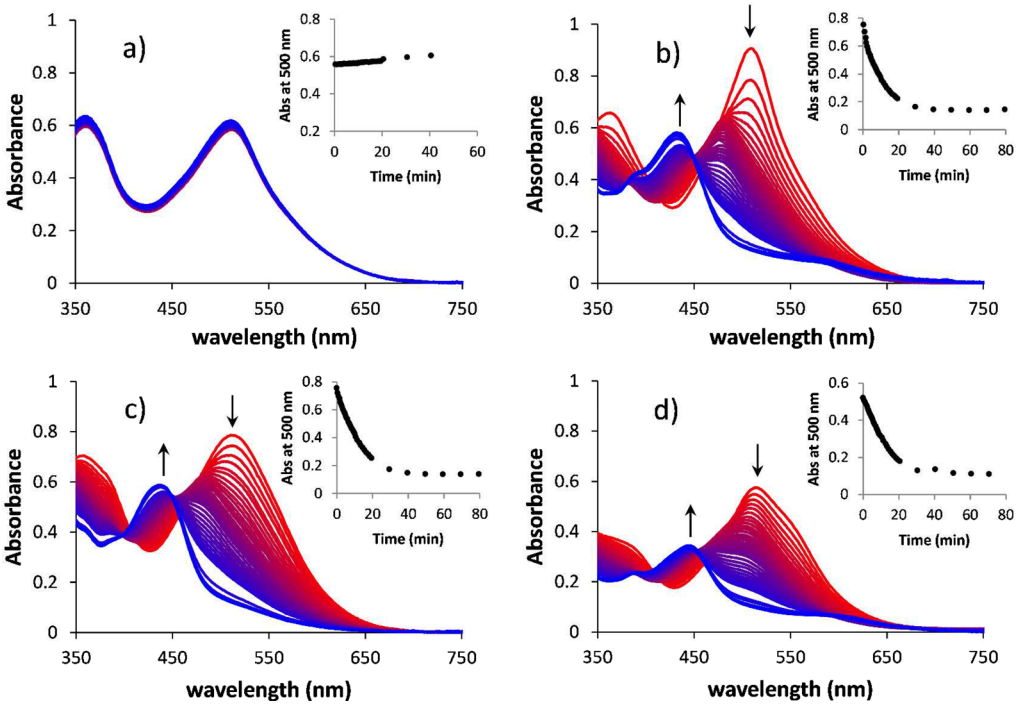

Figure 5. (a) Evolution of the UV−vis spectra of a solution of (a) [**1a**]PF_6 (0.071 mM), (b) [**2a**]PF_6 (0.092 mM), (c) [**2b**]PF_6 (0.121 mM), and (d) [**3a**]PF_6 (0.07 mM) in MeCN upon irradiation under argon with a 493 nm LED at 8.2, 8.3, 7.8, and 8.3 mW·cm^{-2}. The conditions are detailed in Table S2.

of irradiation (Figure 4b). By contrast, no change in the ^{1}H NMR spectrum was observed upon irradiation of [**2b**]PF_6 in the same conditions (Figure 4c). Thus, isomer [**2a**]PF_6, which is a kinetic product formed thermally by the coordination of L-prol to $[Ru(bpy)(dmbpy)(MeCN)_2]^{2+}$, isomerizes photochemically into [**2b**]PF_6, which is the thermodynamically most stable isomer of [**2**]$^+$. According to the UV−vis spectral evolution in Figures 4a and S12b,c, isomerization of [**2a**]$^+$ to [**2b**]$^+$ is not the only process occurring upon irradiation, and photooxidation takes place as well. However, this process occurs at a much slower rate than it does for [**1a**]$^+$.

When a solution of [**2a**]PF_6 in H_2O slowly crystallized in the presence of dimmed daylight, single crystals were obtained that could be analyzed by crystallography. The crystal structure showed a short N5−C26 bond in the proline ligand [1.305(3) Å; Table 1] characteristic of a double N=C bond. Furthermore, the torsion angle C23−N5−C25−C27 was 174.4(2)° in the new crystal (vs 122.1(4)° in the crystal structure of [**2b**]PF_6), which confirmed the quasi-planar geometry of N5 and C26 in the new crystal and thus the oxidation of proline in an imine. In addition, like in [**2b**]$^+$, the carboxylato group was found to be trans to dmbpy, which confirmed the photochemical isomerization of [**2a**]$^+$ to [**2b**]$^+$ during crystallization. Thus, the obtained crystal structure corresponds to the imine complex [**2b**-2H]$^+$. It should be noted that, because this ruthenium complex crystallized in a space group that contained an inversion center ($P\bar{1}$), it is a racemate. Because NMR experiments showed that irradiation of [**2b**]$^+$ did not lead to the Δ isomer [**2d**]$^+$, finding both enantiomers in the crystal structure of $[Ru(dmbpy)(bpy)(L\text{-prol-2H})](PF_6)\cdot H_2O$ means that the Λ-to-Δ racemization occurred after photoisomerization of [**2a**]$^+$ to [**2b**]$^+$ and after photooxidation.

According to Gomez et al., the acidity of the amine of the coordinated L-prol ligand may have a crucial effect on the rate of dehydrogenation for amino acids coordinated to ruthenium polypyridyl complexes.[53] The more acidic the amine is, the faster dehydrogenation takes place. In our case, more methyl substituents on the bpy ligands clearly lead to lower proline photoxidation rates. A plausible interpretation of this observation is that the methyl substituents are electron-donating. More methyl substituents will thus increase the electron density on ruthenium and hence decrease the acidity of the coordinated proline amine. At that stage, however, it remains impossible to say whether or not the steric effects of the methyl groups contribute as well to the dramatic switch in the photoreactivity observed in H_2O between [**2a**]$^+$, [**2b**]$^+$, and [**3a**]$^+$ and the non-hindered complex [**1a**]$^+$.

At that point, the absence of any photosubstitution reaction upon irradiation of all four complexes in an aqueous medium may be surprising because the X-ray structure of [**2b**]$^+$ and the DFT-minimized geometries of the hindered molecules [**2a**]$^+$, [**2b**]$^+$, and [**3a**]$^+$ were distorted enough to suggest low-lying ^{3}MC states. In order to investigate further this question, irradiation was performed in MeCN, which is a much less polar solvent than H_2O, as well as an excellent ligand for ruthenium(II). When an MeCN solution of [**1a**]PF_6 was irradiated at 493 nm under argon, no change in the maximum absorbance of the MLCT was observed (Figure 5a), which confirmed the photostability observed in H_2O. However, when the same experiment was performed using [**2a**]PF_6, [**2b**]PF_6, or [**3a**]PF_6, a clear photoreaction was observed by UV−vis spectroscopy, characterized by a hypsochromic shift of the MLCT band of all three complexes (Figure 5). For the heteroleptic complex [**2a**]$^+$, the maximum absorbance of the ^{1}MLCT band shifted from 509 to 432 nm (Figure 5b), and the MS spectrum after irradiation showed peaks at m/z 185.4, 261.9, 452.2, and 669.2 (Figure S16a). These peaks correspond to the free ligand {6,6′-dmbpy+H}$^+$ (calcd m/z 185.2),

DOI: 10.1021/acs.inorgchem.6b02794
Inorg. Chem. 2017, 56, 4818−4828

$[Ru(bpy)(dmbpy)(MeCN)_2]^{2+}$ (calcd m/z 262.1), $[Ru(bpy)(L\text{-prol-2H})(MeCN)_2]^{+}$ (calcd m/z 452.1), and $\{[Ru(bpy)(dmbpy)(MeCN)_2]PF_6\}^{+}$ (calcd m/z 669.1), respectively. Thus, in MeCN, both bidentate ligands L-prol and dmbpy are photosubstituted by two solvent molecules. Similar results were found when a MeCN solution of $[\mathbf{3a}]PF_6$ was irradiated at 493 nm. A shift in the absorbance maximum of the MLCT band occurred from 516 to 444 nm (Figure 5d), and the MS spectrum after irradiation showed peaks at m/z 185.5, 276.3, 480.2, and 697.2, which corresponded to the free ligand $\{6,6'\text{-dmbpy+H}\}^{+}$ (calcd m/z 185.2), $[Ru(dmbpy)_2(MeCN)_2]^{2+}$ (calcd m/z 276.1), $[Ru(dmbpy)(L\text{-prol-2H})(MeCN)_2]^{+}$ (calcd m/z 480.1), and $\{[Ru(dmbpy)_2(MeCN)_2]PF_6\}^{+}$ (calcd m/z 697.1), respectively (Figure S16b). Thus, also for $[\mathbf{3a}]^{+}$, irradiation in MeCN triggers the non-selective photosubstitution of both the L-prol and dmbpy ligands. When the reaction was performed at a lower light intensity, the photosubstitution rate was lowered and a first isosbestic point at 493 nm could be observed during the first 10 min of the reaction (Figure S19a). A MS spectrum measured at that time point showed no peak corresponding to free dmbpy (Figure S19b), suggesting that L-prol is substituted more rapidly than dmbpy. Overall, in MeCN, the steric strain in the hindered complexes $[\mathbf{2a}]^{+}$ and $[\mathbf{3a}]^{+}$ indeed triggered the expected photosubstitution reactions that were not observed in PBS. However, these photoreactions are not selective and lead to the substitution of both proline and dmbpy.

Considering the discrepancy between the photoreactivity observed in an aqueous buffer and that observed in MeCN, photosubstitution was also studied for $[\mathbf{3a}]^{+}$ in H_2O mixtures containing large amounts (1−80 vol %) of MeCN, thus in pseudo-first-order conditions. As shown in Figure S20, in all cases photosubstitution occurred, as demonstrated by an isosbestic point at 388 nm, two sequential isosbestic points at 457 and at 479 nm showing a two-stage reaction, and the overall shift of the maximum absorbance of the ^{1}MLCT band from 504 to 445 nm. Interestingly, MS spectra measured after the first stage of the reaction showed, next to the peaks at m/z 275.8 and 697.5 corresponding to the final photoproduct $[Ru(dmbpy)_2(MeCN)_2]^{2+}$ (calcd m/z 276.1) and $\{[Ru(dmbpy)_2(MeCN)_2]PF_6\}^{+}$ (calcd m/z 697.1), an additional peak at m/z 313.3 characteristic for an intermediate where one of the bidentate ligands is bound in a monodentate fashion and one MeCN is coordinated, e.g., $\{[Ru(dmbpy)_2(\eta^1\text{-L-prol})(MeCN)]^{2+}\text{+H}\}^{2+}$ (calcd m/z 313.1; Figure S21). MS spectra measured at the steady state did not show this intermediate m/z 313.3 peak or any free dmbpy ligand. Clearly, the two-step photochemical reaction observed by UV−vis corresponds to the initial substitution of one coordinating atom of L-prol by one MeCN ligand, followed by the selective substitution of the second coordinating atom of L-prol by a second MeCN ligand. The absorbance of the solution at 500 nm evolved linearly with the irradiation time during the first 5 min of all experiments, showing that in such conditions the reaction rate was constant (Figure S22a and Table S3). Surprisingly, the observed rate constants (k_{obs}) for formation of the final photoproduct $[Ru(dmbpy)_2(MeCN)_2]^{2+}$ evolved linearly with the MeCN concentrations in H_2O (Figure S22b), which discards a fully dissociative mechanism for such a two-step ligand photosubstitution. Because an associative mechanism is unlikely due to the crowdedness of the strained complex $[\mathbf{3a}]^{+}$, we suggest that photosubstitution may take place via an interchange mechanism, although further kinetic studies should be performed to differenciate between a dissociative interchange and an associative interchange mechanism.[54,55] Overall, an important observation is that the selectivity of the photosubstitution reaction in a 8:2 $MeCN/H_2O$ mixture was different from that observed in pure MeCN: in the former case, photosubstitution was selective and only the proline ligand left the complex, whereas in the latter case, both dmbpy and proline were photosubstituted.

The different photoreactivities of $[\mathbf{2a}]^{+}$, $[\mathbf{2b}]^{+}$, and $[\mathbf{3a}]^{+}$ in PBS, MeCN, and H_2O/MeCN mixtures are puzzling, but they may be rationalized by different hypotheses. First, the coordinating properties of MeCN molecules toward ruthenium(II) are better than those of H_2O. Because photosubstitution of L-prol or dmbpy seems to proceed via intermediates having η^1-coordinated bidentate ligands, more coordinating monodentate ligands may stabilize these intermediates, lower the overall activation barrier, and thus increase the photosubstitution rates in the presence of MeCN. Second, the carboxylate group of L-prol is highly polar, and it has excellent hydrogen-bond-accepting properties. Putative intermediates, where L-prol is coordinated in a η^1,κN fashion, may hence be stabilized in the presence of H_2O, which would enhance the rate of L-prol photosubstitution versus that of dmbpy. In contrast, in MeCN these $[Ru(dmbpy)_2(\eta^1,\kappa\text{N-proline})]^{+}$ intermediates may be comparatively destabilized, while photosubstitution of the less polar dmbpy ligands may occur via stabilized $[Ru(\eta^2\text{-dmbpy})(\eta^2\text{-proline})(\eta^1\text{-dmbpy})(MeCN)]^{+}$ intermediates. Finally, the different triplet excited states involved in the photosubstitution reactions are stabilized to a different extent in polar versus apolar solvents. The ^{3}MLCT states are charge-transfer states that will be stabilized by the solvent with a higher polarity (H_2O), while the ^{3}MC states are not charge-transfer excited states and will be less stabilized by high-polarity solvents. Thus, in H_2O, the ^{3}MLCT−^{3}MC energy gap should be enhanced compared to MeCN, and hence the rate of photosubstitution reactions will be lower. Low photosubstitution rates mean that slow photooxidation and photoisomerization reactions will be observed, whereas in pure MeCN, photosubstititution outcompetes these processes. Thorough—and challenging—theoretical studies, including triplet-state modeling with explicit solvent molecules, will be needed to evaluate the contribution of these three different effects on the solvent dependence of the photosubstitution reactions.

CONCLUSION

In this work, we demonstrated that heteroleptic complexes bearing the N,O-dissymmetric L-prol ligand can be prepared stereoselectively, isolated, and characterized. In complex $[\mathbf{1a}]^{+}$, the absence of steric hindrance and the electron-rich oxygen ligand of proline quench any photosubstitution reaction, both in a chloride-containing aqueous solution and in MeCN. Instead, photooxidation occurs in the presence of air, leading to the formation of a double N=C bond. In parallel, partial isomerization of the ruthenium center from Λ to Δ occurs, as reported for other amino acidato analogues.[24] Increasing the steric strain, as in $[\mathbf{2a}]^{+}$, $[\mathbf{2b}]^{+}$, and $[\mathbf{3a}]^{+}$, did not promote photosubstitution in an aqueous solution (PBS), unlike that demonstrated with other ruthenium complexes such as $[Ru(bpy)_2(dmbpy)]^{2+}$ or $[Ru(tpy)(dmbpy)(L)]^{2+}$.[23,56] In such conditions, increasing the number of methyl groups on the bipyridine ligands strongly slows photooxidation of the

DOI: 10.1021/acs.inorgchem.6b02794
Inorg. Chem. 2017, 56, 4818−4828

proline ligand probably because of the electron-donating effect of the methyl groups. It was necessary to add an excess of MeCN in H_2O to trigger the selective photosubstitution of L-prol in $[\mathbf{3a}]^+$. In pure MeCN, however, the increased strain in $[\mathbf{2a}]^+$, $[\mathbf{2b}]^+$, and $[\mathbf{3a}]^+$ did promote photosubstitution reactions, but two ligands were photosubstituted in a non-selective fashion, i.e., L-prol *and* dmbpy. The influence of the solvent opens interesting mechanistic questions for the photosubstitution reactions of ruthenium polypyridyl complexes. It also increases the complexity of the speciation of light-activatable anticancer compounds in cells. Photosubstitution reactions occurring in cells are usually modeled in aqueous, DCM, or MeCN solutions, without discussing the difference between these media. Our results clearly demonstrate that solvents of different polarities and different coordinating properties may lead to different photoreactivities and that choosing H_2O versus an organic solvent to study photosubstitution is not innocent. Finally, it may be noted that cellular microenvironments such as membranes, DNA, or protein binding pockets are much more hydrophobic than H_2O and that in such microenvironments photoreactions that seem not to occur in H_2O may actually take place.

EXPERIMENTAL SECTION

Materials and Methods. The ligands 2,2′-bipyridine (bpy), 6,6′-dimethyl-2,2′-bipyridine (dmbpy), and L-proline (L-prol), as well as monopotassium phosphate (KH_2PO_4), sodium chloride (NaCl), and *cis*-bis(2,2′-bipyridine)dichlororuthenium(II) hydrate [*cis*-Ru(bpy)$_2$Cl$_2$], were purchased from Sigma-Aldrich. Lithium chloride (LiCl) and potassium hexafluorophosphate (KPF_6) were purchased from Alfa-Aesar, and potassium carbonate (K_2CO_3) was obtained from Merck. $RuCl_3 \cdot 3H_2O$ was provided by Prof. Dr. E. Bouwman. All reactants and solvents were used without further purification. The syntheses of *cis*-[Ru(dmbpy)$_2$Cl$_2$] ([**4**]) and [**1**]PF_6 were carried out according to literature procedures.[34,57] Size-exclusion chromatography was performed using Sephadex LH-20.

Electrospray mass spectrometry (ES MS) spectra were recorded using a Thermoquest Finnagen AQA spectrometer and a MSQ Plus spectrometer, and CD spectra were recorded using a Bio-Logic MOS-500 spectrometer with a Bio-Logic ALX-300 lamp. For irradiation experiments of NMR tubes, the light of a LOT 1000 W xenon arc lamp mounted with an IR filter and either a 400 nm long-pass or a 450 nm 450FS10-50 filter from Andover Corp. was used. UV−vis experiments were performed on a Cary Varian spectrometer. When following photoreactions by UV−vis, MS, or CD, a light-emitting-diode (LED) light source (λ_{ex} = 493 nm, with a full width at half-maximum of 14 nm) with a light intensity between 8.0 and 11.5 mW·cm^{-2} was used. For spectroelectrochemistry, UV−vis-light-source Avantes-DH-S-BAL and Avantes Avaspec-2048 spectrometers were used. An Autolab PGSTAT101 potentiostat was used to perform chronoamperometry.

All ^{1}H NMR spectra were recorded on a Bruker DPX-300 or DMX-400 spectrometer. Chemical shifts are indicated in parts per million relative to the residual solvent peak. For NMR experiments under argon, NMR tubes with polytetrafluoroethylene stoppers were used. For some NMR reactions, deuterated PBS was used as the solvent. A 10 mM PBS with 110 mM NaCl was prepared by dissolving KH_2PO_4 (6.5 mg, 0.047 mmol), K_2HPO_4 (36.8 mg, 0.211 mmol), and NaCl (160.8 mg, 2.752 mmol) in D_2O (25 mL) to reach a final pH of 7.54 at 22 °C. The pH was measured with a pH meter, taking into account that the measured pD = pH + 0.4.[58] For the rest of the irradiations followed by UV−vis, MS, or CD, a 10 mM PBS with 110 mM NaCl was prepared by dissolving KH_2PO_4 (64.3 mg, 0.472 mmol), K_2HPO_4 (353.6 mg, 2.030 mmol), and NaCl (1.605 g, 27.464 mmol) in Milli-Q H_2O (250 mL) to reach a final pH of 7.35 at 22 °C.

Syntheses. *[Ru(bpy)$_2$(L-prol-2H)]PF_6 ([**7**]PF_6).* The synthesis of complex [**7**]PF_6 was adapted from a literature procedure.[50] Complex [**1a**]PF_6 (3.0 mg, 0.005 mmol) was dissolved in 50 mL of PBS (pH 7.35) and transferred to one of the compartments of the cell. Oxidation at a constant potential of +0.645 V versus Ag/AgCl reference electrode was carried out under argon in a two-compartment cell with a Nafion membrane. Carbon sponge electrodes were used as working and counter electrodes. Electrolysis was continued until the current remained stable. Then, complex [**7**]PF_6 was extracted with DCM (3 × 20 mL) and dried over $MgSO_4$. After evaporation of the solvent by reduced pressure, an orange solid was obtained (2.8 mg, 93%). ^{1}H NMR (300 MHz, methanol-d_4): δ 8.72 (d, J = 5.6 Hz, 1H), 8.66 (d, J = 8.1 Hz, 2H), 8.59−8.50 (m, 3H), 8.21 (dtd, J = 12.1, 7.9, and 1.5 Hz, 2H), 7.97−7.70 (m, 5H), 7.57 (d, J = 5.8 Hz, 1H), 7.33−7.20 (m, 2H), 3.88 (s, 1H), 3.20−3.02 (m, 1H), 2.97−2.79 (m, 1H), 2.30 (m, J = 3.4 Hz, 1H), 2.05 (m, 1H). ES MS (calcd): m/z 526.2 (526.1).

*rac-[Ru(bpy)(dmbpy)$_2$](PF_6)$_2$ ([**5**](PF_6)$_2$).* Ligand bpy (35.2 mg, 0.225 mmol, 0.8 equiv) and [**4**] (149.7 mg, 0.278 mmol) were dissolved in ethylene glycol (5 mL), and the solution was degassed by bubbling argon for 30 min in a pressure tube. The tube was closed, put in a preheated oven at 190 °C for 3.5 h, and then cooled to room temperature. After the addition of H_2O (10 mL) and a saturated KPF_6 aqueous solution (0.5 mL), an orange precipitate was obtained. The suspension was filtered, and the precipitate was washed with cold H_2O and cold ethanol. After drying under air, an orange powder was obtained (201 mg, 79%), which shows traces of ligand scrambling. ^{1}H NMR (300 MHz, MeCN-d_3): δ 8.46 (d, J = 8.0 Hz, 2H), 8.29 (d, J = 7.8 Hz, 2H), 8.14 (q, J = 8.3 Hz, 4H), 7.91 (td, J = 8.0 and 1.4 Hz, 2H), 7.86 (d, J = 5.2 Hz, 2H), 7.72 (t, J = 7.9 Hz, 2H), 7.51−7.46 (m, 2H), 7.34 (ddd, J = 7.4, 5.9, and 1.3 Hz, 2H), 7.07 (dd, J = 7.8 and 0.9 Hz, 2H), 1.79 (s, 6H), 1.68 (s, 6H). ^{13}C NMR (75 MHz, MeCN-d_3): δ 167.80, 166.08, 160.54, 159.42, 158.52, 153.31, 139.49, 138.93, 138.15, 129.04, 128.18, 127.97, 124.56, 124.20, 123.52, 26.40, 25.45. ES MS (calcd): m/z 313.5 (313.1, [M − 2PF_6]$^{2+}$), 771.4 (771.1, [M − PF_6]$^+$).

*rac-[Ru(bpy)(dmbpy)(MeCN)$_2$](PF_6)$_2$ ([**6**](PF_6)$_2$).* [**5**](PF_6)$_2$ (150.1 mg, 0.164 mmol) was dissolved in a preparative irradiation cell in MeCN (110 mL). After the mixture was degassed by bubbling argon for 20 min, the orange solution was irradiated with the beam of a 1000 W xenon lamp with both IR and UV cutoff filters. After 2 h of irradiation, the solvent was removed under reduced pressure. The orange solid was redissolved in MeOH and purified by size-exclusion chromatography in MeOH to remove free dmbpy ligand. After solvent evaporation, an orange solid was obtained (84 mg, 59%). ^{1}H NMR (300 MHz, MeCN-d_3): δ 9.39 (ddd, J = 5.6, 1.5, and 0.7 Hz, 1H), 8.38 (dt, J = 8.1 and 1.1 Hz, 1H), 8.27 (dt, J = 8.0 and 1.0 Hz, 2H), 8.20 (td, J = 7.9 and 1.5 Hz, 1H), 8.14−8.06 (m, 2H), 7.93 (td, J = 7.9 and 1.5 Hz, 1H), 7.82−7.66 (m, 4H), 7.52 (ddd, J = 5.7, 1.6, and 0.8 Hz, 1H), 7.31 (ddd, J = 7.4, 5.7, and 1.4 Hz, 1H), 7.12 (dd, J = 7.7 and 1.3 Hz, 1H), 2.47 (s, 3H), 1.84 (s, 3H). ^{13}C NMR (75 MHz, MeCN-d_3): δ 167.33, 167.06, 159.84, 159.52, 159.39, 158.51, 155.64, 153.34, 139.36, 139.29, 138.87, 138.74, 128.30, 128.05, 127.97, 127.69, 124.64, 124.34, 122.53, 121.91, 27.23, 25.26, 4.74. ES MS (calcd): m/z 262.3 (262.1, [M − 2PF_6]$^{2+}$), 669.2 (669.1, [M − PF_6]$^+$).

*Λ-[Ru(bpy)(dmbpy)(L-prol)]PF_6 ([**2**]PF_6).* L-prol (25.0 mg, 0.217 mmol, 2.5 equiv), K_2CO_3 (15.0 mg, 0.108 mmol, 1.25 equiv), and [**6**](PF_6)$_2$ (70.0 mg, 0.086 mmol) were dissolved in ethylene glycol (5 mL) and degassed by bubbling argon for 20 min in a pressure tube. The tube was closed and put in a preheated oven at 190 °C. After 40 min at 190 °C, the reaction mixture was cooled to room temperature, and most of the solvent was removed under high vacuum at 40 °C. Then, the dark-red paste was dissolved in H_2O (15 mL) and extracted with DCM (3 × 10 mL). The organic phases were combined and dried over $MgSO_4$, which was filtered. The solvent was then evaporated under reduced pressure, and the solid was purified by an alumina chromatography column using a mixture of 99:1 DCM/MeOH as the eluent. Two main fractions were obtained from a long band (with an R_f around 0.35), which corresponded to the diastereoisomers [**2a**]PF_6 and [**2b**]PF_6.

[**2a**]PF_6 (red solid, 18.5 mg, 31%) was isolated as 85% pure containing traces of [**3**]PF_6, as shown by ^{1}H NMR (Figure S3) and

DOI: 10.1021/acs.inorgchem.6b02794
Inorg. Chem. 2017, 56, 4818−4828

MS. ^{1}H NMR (500 MHz, D_2O): δ 8.76 (d, J = 5.6 Hz, 1H, D6), 8.73 (d, J = 5.7 Hz, 1H, C6), 8.52 (d, J = 8.1 Hz, 1H, D3), 8.41 (d, J = 8.2 Hz, 1H, C3), 8.22 (d, J = 8.1 Hz, 1H, A3), 8.14−8.09 (m, 2H, B3, D4), 7.96 (t, J = 8.0 Hz, 1H, A4), 7.85 (t, J = 8.0 Hz, 1H, C4), 7.70 (t, J = 7.9 Hz, 1H, B4), 7.67−7.63 (m, 1H, D5), 7.53 (d, J = 7.7 Hz, 1H, A5), 7.30 (td, J = 6.4, 5.8, and 1.2 Hz, 1H, C5), 7.01 (d, J = 7.6 Hz, 1H, B5), 2.98 (s, 3H, AMe), 2.03 (q, J = 10.1 Hz, 1H, P3), 1.93 (dd, J = 11.2 and 5.6 Hz, 1H, P5), 1.54 (td, J = 13.2, 12.1, and 6.5 Hz, 1H, P3), 1.46 (dt, J = 13.1 and 6.3 Hz, 1H, P4), 1.20 (s, 4H), 1.14 (tt, J = 11.3 and 5.6 Hz, 1H, P5). ES MS (calcd): m/z 556.1 (556.1, $[M - PF_6]^+$), 584.0 (584.1, $[3]^+$).

[**2b**]PF_6 (pure red solid, 8.1 mg, 13%). ^{1}H NMR (300 MHz, D_2O): δ 9.11 (d, J = 5.6 Hz, 1H, D6), 8.53 (d, J = 8.2 Hz, 1H, D3), 8.43 (d, J = 8.2 Hz, 1H, C3), 8.31 (d, J = 8.1 Hz, 1H, A3), 8.20 (d, J = 8.0 Hz, 1H, B3), 8.10 (q, J = 5.8 and 5.3 Hz, 2H, C6/D4), 8.00 (t, J = 7.9 Hz, 1H, A4), 7.89 (dt, J = 7.8 and 1.5 Hz, 1H, C4), 7.74−7.66 (m, 2H, A4/D5), 7.60 (d, J = 7.7 Hz, 1H, A5), 7.23 (ddd, J = 7.3, 5.7, and 1.3 Hz, 1H, C5), 7.08 (d, J = 7.6 Hz, 1H, B5), 6.09−5.96 (m, 1H), 4.08 (q, J = 8.9 Hz, 1H), 2.55 (s, 4H), 2.23 (td, J = 10.0 and 5.8 Hz, 1H), 1.62 (s, 3H), 1.55−1.34 (m, 2H), 1.30−1.16 (m, 1H). ES MS (calcd): m/z 556.1 (556.1, $[M - PF_6]^+$). UV−vis [λ, nm (ε, $M^{-1}\cdot cm^{-1}$)]: 511 (12300) in pure acetonitrile; 497 (9460) in PBS.

Λ-*[Ru(dmbpy)$_2$(L-prol)]PF_6 ([**3a**]PF_6).* L-prol (22.1 mg, 0.192 mmol, 2.2 equiv), K_2CO_3 (13.2 mg, 0.094 mmol, 1.1 equiv), and [**4**] (47.5 mg, 0.088 mmol) were dissolved in ethylene glycol (1 mL) and degassed by bubbling argon for 20 min in a pressure tube. The tube was closed and put in a preheated oven at 190 °C, and after 45 min, the mixture was cooled to room temperature. After the addition of H_2O (4 mL) and a saturated KPF_6 aqueous solution (0.5 mL), a red precipitate was obtained. The suspension was filtered, and the solid was washed with cold H_2O and cold diethyl ether. The red solid was purified by size-exclusion chromatography in MeOH, obtaining a pure red solid (36 mg, 56%). ^{1}H NMR (300 MHz, methanol-d_4): δ 8.45−8.35 (m, 3H, D3, A3, C3), 8.33 (d, J = 8.0 Hz, 1H, B3), 8.01 (q, J = 8.1 Hz, 2H, A4, D4), 7.85 (td, J = 7.9 and 1.9 Hz, 2H, B4, C4), 7.57−7.49 (m, 2H, D3, A5), 7.37 (dd, J = 7.5 and 0.6 Hz, 1H, C5), 7.26 (d, J = 7.5 Hz, 1H, B5), 3.43−3.35 (m, 1H, P2), 2.88 (s, 3H, AMe), 2.48 (s, 3H, DMe), 2.14 (m, 1H, P5), 2.00 (s + m, 4H, CMe, P3), 1.66 (s + m, 4H, BMe, P3), 1.46 (m, 1H, P4), 1.34 (m, 1H, P4), 0.78 (qd, J = 11.4 and 6.0 Hz, 1H, P5). High-resolution ES MS (calcd): m/z 584.15951 (584.16018, $[M - PF_6]^+$). Anal. Calcd for $C_{29}H_{32}F_6N_5O_2PRu$: C, 47.80; H, 4.43; N, 9.61. Found: C, 47.13; H, 4.41; N, 9.45. UV−vis [λ, nm (ε, $M^{-1}\cdot cm^{-1}$)]: 515 (7660) in pure MeCN.

Crystals Growth and X-ray Structure. *Complex [**2b**]PF_6.* Crystal growth: [**2b**]PF_6 (2.0 mg, 0.003 mmol) was dissolved in H_2O (0.7 mL) in a GC vial. After 2 weeks, single crystals suitable for X-ray diffraction were obtained.

X-ray structure: All reflection intensities were measured at 110(2) K using a SuperNova diffractometer (equipped with an Atlas detector) with Mo Kα radiation (λ = 0.71073 Å) under the program *CrysAlisPro* (version 1.171.36.32, Agilent Technologies, 2013). The temperature of the data collection was controlled using a Cryojet system (manufactured by Oxford Instruments). The *CrysAlisPro* program was used to refine the cell dimensions and for data reduction. The structure was solved by direct methods with *SHELXS-2014/7* (Sheldrick, 2015) and was refined on F^2 with *SHELXL-2014/7* (Sheldrick, 2015). Analytical numeric absorption correction based on a multifaceted crystal model was applied using *CrysAlisPro*. The hydrogen atoms were placed at calculated positions (unless otherwise specified) using the instructions AFIX 13, AFIX 23, AFIX 43, or AFIX 137 with isotropic displacement parameters having values of 1.2 or 1.5 U_{eq} of the attached carbon or nitrogen atoms. The hydrogen atoms attached to O1W and O2W were found from a difference Fourier map, and their coordinates were refined freely. The DFIX restraints were used to keep the OH and H···H distances within acceptable ranges. The structure is partly disordered.

Additional notes: (i) The asymmetric unit contains two crystallographically independent ruthenium molecules, two PF_6^- counterions, and two lattice H_2O solvent molecules. (ii) Both PF_6^- counterions are disordered over two orientations, and the occupancy factors of the major components of the disorder refine to 0.52(3) and 0.777(9). (iii) The structure refines in the space group $P1$. The absolute configuration is established by anomalous dispersion effects in diffraction measurements on the crystal. The Flack parameter refines to −0.013(12).

*Oxidized Complex [**2b**-2H]PF_6.* Crystal growth: [**2a**]PF_6 (2.0 mg, 0.003 mmol) was dissolved in H_2O (0.7 mL) in a GC vial and left in dimmed daylight. After 6 weeks, single crystals suitable for X-ray diffraction were obtained.

X-ray structure: All reflection intensities were measured at 110(2) K using a SuperNova diffractometer (equipped with an Atlas detector) with Cu Kα radiation (λ = 1.54178 Å) under the program *CrysAlisPro* (version 1.171.36.32, Agilent Technologies, 2013). The same program was used to refine the cell dimensions and for data reduction. The structure was solved with the program *SHELXS-2014/7* (Sheldrick, 2015) and was refined on F^2 with *SHELXL-2014/7* (Sheldrick, 2015). Analytical numeric absorption correction using a multifaceted crystal model was applied using *CrysAlisPro*. The temperature of the data collection was controlled using a Cryojet system (manufactured by Oxford Instruments). The hydrogen atoms were placed at calculated positions (unless otherwise specified) using the instructions AFIX 23, AFIX 43, or AFIX 137 with isotropic displacement parameters having values of 1.2 or 1.5 of the attached carbon atoms. The deuterium atoms attached to O1W were found from difference Fourier maps, and their coordinates were refined freely. The structure is ordered.

Irradiation Experiments Followed by ^{1}H NMR. *Irradiation of [**1a**](PF_6).* A stock solution of [**1a**]PF_6 in deuterated PBS (1.5 mg, 5 mL, 0.045 mM) was prepared and degassed under argon. Then, 650 μL were transferred, under argon, to a NMR tube. The tube was irradiated at 310 K with a LOT 1000 W xenon lamp equipped with IR short-pass and >400 nm long-pass filters. In addition, a control experiment without white-light irradiation was performed, in which no reaction was observed after 5 h. The reactions were monitored by ^{1}H NMR at various time intervals.

*Irradiation of [**2a**](PF_6) and [**2b**](PF_6).* [**2a**](PF_6) (2.7 mg) and [**2b**](PF_6) (2.6 mg) were weighed in two NMR tubes and dissolved in D_2O (0.7 mL in each tube). The tubes were irradiated at room temperature with a 1000 W xenon lamp equipped with a 450 nm blue-light 450FS10-50 filter from Andover Corp. In addition, a control experiment without white-light irradiation was performed, in which no reaction was observed after 5 h. The reactions were monitored by ^{1}H NMR at various time intervals.

Irradiation Experiments Followed by MS, UV−vis, and CD. UV−vis spectroscopy was performed using a UV−vis spectrometer equipped with the temperature control set to 298 K and a magnetic stirrer. The irradiation experiments were performed in a quartz cuvette containing 3 mL of a solution. A stock solution of the desired complex was prepared using either MeCN or PBS, which was then diluted in the cuvette to a working solution concentration. When the experiment was carried under argon, the sample was degassed 15 min by gentle bubbling of argon and the atmosphere was kept inert during the experiment by a gentle flow of argon on top of the cuvette. A UV−vis spectrum was measured every 30 s for the first 10 min, every 1 min for the next 10 min, and eventually every 10 min until the end of the experiment. Data were analyzed with Microsoft Excel. The quantum yield for the photooxidation of [**1a**]PF_6 in PBS was calculated by modeling the time evolution of the absorbance spectrum of the solution using the *Glotaran* software (Figure S14).[59] The experimental conditions are detailed in Table S2.

Spectroelectrochemistry. A solution of [**1a**]PF_6 in PBS (0.1 mM) was transferred into the working compartment of a two-compartment cell separated by a Nafion membrane, whereas the countercompartment contained only PBS. Carbone sponges with a resistance lower than 10 mΩ were used as working and counter electrodes. A Ag/AgCl electrode was used as the reference electrode. Once the solution was degassed by bubbling argon for 15 min, the UV−vis probe was submerged in the working solution. Chronoamperometry was performed at a constant potential of +0.645 V vs Ag/AgCl reference electrode, taking points every second, while UV−vis

DOI: 10.1021/acs.inorgchem.6b02794
Inorg. Chem. 2017, 56, 4818−4828

spectra were recorded every 2 min. When the current of the chronoamperometry was constant, the experiment was terminated.

DFT Calculations. Electronic structure calculations were performed using DFT, as implemented in the ADF program (SCM). The structures of all possible isomers of $[\mathbf{1}]^+$, $[\mathbf{2}]^+$, and $[\mathbf{3}]^+$ were optimized first in vacuum and then in H_2O using COSMO to simulate the effect of the solvent. The PBE0 functional and a triple-ζ potential basis set (TZP) were used for all calculations.

■ ASSOCIATED CONTENT

Supporting Information

The Supporting Information is available free of charge on the ACS Publications website at DOI: 10.1021/acs.inorgchem.6b02794.

^{1}H NMR, MS, and CD spectra of $[\mathbf{1a}]PF_6$, $[\mathbf{2a}]PF_6$, $[\mathbf{2b}]PF_6$, and $[\mathbf{3a}]PF_6$, crystal growth and X-ray structures, UV−vis, MS, CD, and ^{1}H NMR spectra of the irradiation of $[\mathbf{1a}]PF_6$, $[\mathbf{2a}]PF_6$, $[\mathbf{2b}]PF_6$, $[\mathbf{3a}]PF_6$, spectroelectrochemistry of $[\mathbf{1a}]PF_6$, DFT calculations, and Cartesian coordinates (PDF)

X-ray crystallographic data in CIF format (CIF)

X-ray crystallographic data in CIF format (CIF)

■ AUTHOR INFORMATION

Corresponding Author

*E-mail: bonnet@chem.leidenuniv.nl.

ORCID

Sylvestre Bonnet: 0000-0002-5810-3657

Notes

The authors declare no competing financial interest.

■ ACKNOWLEDGMENTS

The European Research Council is acknowledged for a Starting grant to S.B. The Netherlands Organization for Scientific Research is acknowledged for a VIDI grant to S.B. Prof. Elisabeth Bouwman is kindly ackowledged for scientific discussion and support.

■ REFERENCES

(1) Bonnet, S.; Collin, J. P.; Koizumi, M.; Mobian, P.; Sauvage, J. P. Transition-Metal-Complexed Molecular Machine Prototypes. *Adv. Mater.* **2006**, *18*, 1239−1250.

(2) Champin, B.; Mobian, P.; Sauvage, J.-P. Transition metal complexes as molecular machine prototypes. *Chem. Soc. Rev.* **2007**, *36*, 358−366.

(3) Sauvage, J.; Collin, J.; Chambron, J.; Guillerez, S.; Coudret, C.; Balzani, V.; Barigelletti, F.; De Cola, L.; Flamigni, L. ruthenium(II) and osmium(II) bis(terpyridine) complexes in covalently-linked multicomponent systems - synthesis, electrochemical behaviour, absorption spectra, and photochemical and photophysical properties. *Chem. Rev.* **1994**, *94*, 993−1019.

(4) Balzani, V.; Bergamini, G.; Marchioni, F.; Ceroni, P. Ru(II)-bipyridine complexes in supramolecular systems, devices and machines. *Coord. Chem. Rev.* **2006**, *250*, 1254−1266.

(5) Balzani, V.; Ceroni, P.; Juris, A.; Venturi, M.; Campagna, S.; Puntoriero, F.; Serroni, S. Dendrimers based on photoactive metal complexes. Recent advances. *Coord. Chem. Rev.* **2001**, *219-221*, 545−572.

(6) Balzani, V.; Credi, A.; Venturi, M. Light powered molecular machines. *Chem. Soc. Rev.* **2009**, *38*, 1542−1550.

(7) Fernandez-Moreira, V.; Thorp-Greenwood, F. L.; Coogan, M. P. Application of d6 transition metal complexes in fluorescence cell imaging. *Chem. Commun.* **2010**, *46*, 186−202.

(8) Martin, A.; Byrne, A.; Burke, C. S.; Forster, R. J.; Keyes, T. E. Peptide-Bridged Dinuclear Ru(II) Complex for Mitochondrial Targeted Monitoring of Dynamic Changes to Oxygen Concentration and ROS Generation in Live Mammalian Cells. *J. Am. Chem. Soc.* **2014**, *136*, 15300−15309.

(9) Gill, M. R.; Garcia-Lara, J.; Foster, S. J.; Smythe, C.; Battaglia, G.; Thomas, J. A. A ruthenium(II) polypyridyl complex for direct imaging of DNA structure in living cells. *Nat. Chem.* **2009**, *1*, 662−667.

(10) Gill, M. R.; Thomas, J. A. Ruthenium(ii) polypyridyl complexes and DNA-from structural probes to cellular imaging and therapeutics. *Chem. Soc. Rev.* **2012**, *41*, 3179−3192.

(11) Blackmore, L.; Moriarty, R.; Dolan, C.; Adamson, K.; Forster, R. J.; Devocelle, M.; Keyes, T. E. Peptide directed transmembrane transport and nuclear localization of Ru(ii) polypyridyl complexes in mammalian cells. *Chem. Commun.* **2013**, *49*, 2658−2660.

(12) Lee, J.; Udugamasooriya, D. G.; Lim, H.-S.; Kodadek, T. Potent and selective photo-inactivation of proteins with peptoid-ruthenium conjugates. *Nat. Chem. Biol.* **2010**, *6*, 258−260.

(13) Lee, J. Y.; Yu, P.; Xiao, X. S.; Kodadek, T. A general system for evaluating the efficiency of chromophore-assisted light inactivation (CALI) of proteins reveals Ru(II) tris-bipyridyl as an unusually efficient "warhead". *Mol. BioSyst.* **2008**, *4*, 59−65.

(14) Prakash, J.; Kodanko, J. J. Metal-based methods for protein inactivation. *Curr. Opin. Chem. Biol.* **2013**, *17*, 197−203.

(15) Mari, C.; Pierroz, V.; Ferrari, S.; Gasser, G. Combination of Ru (II) complexes and light: new frontiers in cancer therapy. *Chem. Sci.* **2015**, *6*, 2660−2686.

(16) Hufziger, K. T.; Thowfeik, F. S.; Charboneau, D. J.; Nieto, I.; Dougherty, W. G.; Kassel, W. S.; Dudley, T. J.; Merino, E. J.; Papish, E. T.; Paul, J. J. Ruthenium dihydroxybipyridine complexes are tumor activated prodrugs due to low pH and blue light induced ligand release. *J. Inorg. Biochem.* **2014**, *130*, 103−111.

(17) Lopes-dos-Santos, V.; Campi, J.; Filevich, O.; Ribeiro, S.; Etchenique, R. In vivo photorelease of GABA in the mouse cortex. *Braz. J. Med. Biol. Res.* **2011**, *44*, 688−693.

(18) Mosquera, J.; Sanchez, M. I.; Mascarenas, J. L.; Eugenio Vazquez, M. Synthetic peptides caged on histidine residues with a bisbipyridyl ruthenium(ii) complex that can be photolyzed by visible light. *Chem. Commun.* **2015**, *51*, 5501−5504.

(19) Hidayatullah, A. N.; Wachter, E.; Heidary, D. K.; Parkin, S.; Glazer, E. C. Photoactive Ru(II) Complexes With Dioxinophenanthroline Ligands Are Potent Cytotoxic Agents. *Inorg. Chem.* **2014**, *53*, 10030.

(20) Garner, R. N.; Gallucci, J. C.; Dunbar, K. R.; Turro, C. [Ru(bpy)(2)(5-cyanouracil)2]2+ as a Potential Light-Activated Dual-Action Therapeutic Agent. *Inorg. Chem.* **2011**, *50*, 9213−9215.

(21) Chen, Y.; Lei, W.; Jiang, G.; Hou, Y.; Li, C.; Zhang, B.; Zhou, Q.; Wang, X. Fusion of photodynamic therapy and photoactivated chemotherapy: a novel Ru(ii) arene complex with dual activities of photobinding and photocleavage toward DNA. *Dalton Trans.* **2014**, *43*, 15375−15384.

(22) Sainuddin, T.; Pinto, M.; Yin, H.; Hetu, M.; Colpitts, J.; McFarland, S. A. Strained ruthenium metal−organic dyads as photocisplatin agents with dual action. *J. Inorg. Biochem.* **2016**, *158*, 45−54.

(23) Howerton, B. S.; Heidary, D. K.; Glazer, E. C. Strained Ruthenium Complexes Are Potent Light-Activated Anticancer Agents. *J. Am. Chem. Soc.* **2012**, *134*, 8324−8327.

(24) Vagg, R. S.; Williams, P. A. Chiral metal complexes 2. Light-catalysed diastereoisomeric equilibration in aqueous solutions of cis-[Ru(phen)2(L-serine)]+ and its 2,2′-bipyridyl analogue. *Inorg. Chim. Acta* **1981**, *52*, 69−72.

(25) Vagg, R. S.; Williams, P. A. Chiral metal complexes. 1. Photochemical inversion in ternary Ru(II) complexes of diimines and L-tryptophane. *Inorg. Chim. Acta* **1981**, *51*, 61−65.

(26) Leane, D.; Keyes, T. E. Electronic coupling and photochemical stability of O,N bound mononuclear Ru(II) and Os(II) − Hydroquinone complexes. *Inorg. Chim. Acta* **2006**, *359*, 1627−1636.

DOI: 10.1021/acs.inorgchem.6b02794
Inorg. Chem. 2017, 56, 4818−4828

(27) Keyes, T. E.; Vos, J. G.; Kolnaar, J. A.; Haasnoot, J. G.; Reedijk, J.; Hage, R. Tuning of the photostability of bis(2,2′-biquinoline)-ruthenium(II) complexes containing pyridyltriazole ligands by variation of pH. *Inorg. Chim. Acta* **1996**, *245*, 237−242.
(28) Heidary, D. K.; Howerton, B. S.; Glazer, E. C. Coordination of Hydroxyquinolines to a Ruthenium Bis-dimethyl-phenanthroline Scaffold Radically Improves Potency for Potential as Antineoplastic Agents. *J. Med. Chem.* **2014**, *57*, 8936−8946.
(29) Sun, Q.; Mosquera-Vazquez, S.; Lawson Daku, L. M.; Guénée, L.; Goodwin, H. A.; Vauthey, E.; Hauser, A. Experimental Evidence of Ultrafast Quenching of the 3MLCT Luminescence in Ruthenium(II) Tris-bipyridyl Complexes via a 3dd State. *J. Am. Chem. Soc.* **2013**, *135*, 13660−13663.
(30) Knof, U.; von Zelewsky, A. Predetermined chirality at metal centers. *Angew. Chem., Int. Ed.* **1999**, *38*, 302−322.
(31) Gong, L.; Mulcahy, S. P.; Harms, K.; Meggers, E. Chiral-Auxiliary-Mediated Asymmetric Synthesis of Tris-Heteroleptic Ruthenium Polypyridyl Complexes. *J. Am. Chem. Soc.* **2009**, *131*, 9602−9603.
(32) Hesek, D.; Inoue, Y.; Everitt, S. R. L.; Ishida, H.; Kunieda, M.; Drew, M. G. R. Conversion of a new chiral reagent Δ-[Ru(bpy)$_2$(dmso)Cl]PF$_6$ to Δ-[Ru(bpy)$_2$(dmbpy)]PF$_6$Cl with 96.8% retention of chirality (dmbpy = 4,4[prime or minute]-dimethyl-2,2[prime or minute]-bipyridine). *Chem. Commun. (Cambridge, U. K.)* **1999**, *0*, 403−404.
(33) Hayoz, P.; Von Zelewsky, A.; Stoeckli-Evans, H. Stereoselective synthesis of octahedral complexes with predetermined helical chirality. *J. Am. Chem. Soc.* **1993**, *115*, 5111−5114.
(34) Fu, C.; Wenzel, M.; Treutlein, E.; Harms, K.; Meggers, E. Proline as Chiral Auxiliary for the Economical Asymmetric Synthesis of Ruthenium(II) Polypyridyl Complexes. *Inorg. Chem.* **2012**, *51*, 10004−10011.
(35) Goodwin, T. J.; Williams, P. A.; Stephens, F. S.; Vagg, R. S. Chiral metal complexes. 12. Chiroptical, 1H NMR and crystallographic studies of the diastereoisomers Λ- and Δ-[Ru(diimine)2(S-threonine)]+ and their S-allothreonine analogues. *Inorg. Chim. Acta* **1984**, *88*, 165−181.
(36) Goodwin, T. J.; Williams, P. A.; Vagg, R. S. Chiral metal complexes. 5. Sources of chiral discrimination in aqueous solutions of the complexes Δ,Λ-[Ru(diimine)2(L-aspartate)]° and their conjugate acids. *Inorg. Chim. Acta* **1982**, *63*, 133−140.
(37) Burke, C. S.; Keyes, T. E. An efficient route to asymmetrically diconjugated tris(heteroleptic) complexes of Ru(II). *RSC Adv.* **2016**, *6*, 40869−40877.
(38) Mulhern, D.; Brooker, S.; Gorls, H.; Rau, S.; Vos, J. G. Synthesis of mononuclear and dinuclear ruthenium(ii) tris(heteroleptic) complexes via photosubstitution in bis(carbonyl) precursors. *Dalton Trans.* **2006**, 51−57.
(39) Freedman, D. A.; Evju, J. K.; Pomije, M. K.; Mann, K. R. Convenient Synthesis of Tris-Heteroleptic Ruthenium(II) Polypyridyl Complexes. *Inorg. Chem.* **2001**, *40*, 5711−5715.
(40) Myahkostupov, M.; Castellano, F. N. Synthesis and Characterization of Tris(Heteroleptic) Ru(II) Complexes Bearing Styryl Subunits. *Inorg. Chem.* **2011**, *50*, 9714−9727.
(41) Spiccia, L.; Deacon, G. B.; Kepert, C. M. Synthetic routes to homoleptic and heteroleptic ruthenium(II) complexes incorporating bidentate imine ligands. *Coord. Chem. Rev.* **2004**, *248*, 1329−1341.
(42) Anderson, P. A.; Deacon, G. B.; Haarmann, K. H.; Keene, F. R.; Meyer, T. J.; Reitsma, D. A.; Skelton, B. W.; Strouse, G. F.; Thomas, N. C. Designed Synthesis of Mononuclear Tris(heteroleptic) Ruthenium Complexes Containing Bidentate Polypyridyl Ligands. *Inorg. Chem.* **1995**, *34*, 6145−6157.
(43) von Zelewsky, A.; Gremaud, G. Ruthenium(II) complexes with 3 different diimine ligands. *Helv. Chim. Acta* **1988**, *71*, 1108−1115.
(44) Bosnich, B. Exciton circular dichroism and the absolute configurations of molecules containing nonidentical chromophores. Bis (o-phenanthroline)-2,2′-bipyridylruthenium(II) and bis(2,2′-bipyridyl)-o-phenanthrolineruthenium(II) ions. *Inorg. Chem.* **1968**, *7*, 2379−2386.
(45) Bosnich, B. Absolute configurations of bis-bidentate chelate compounds. The case of the cis-bis(pyridine)bis(o-phenanthroline)-ruthenium(II) ion. *Inorg. Chem.* **1968**, *7*, 178−180.
(46) Robinson, K.; Gibbs, G. V.; Ribbe, P. H. Quadratic Elongation: A Quantitative Measure of Distortion in Coordination Polyhedra. *Science* **1971**, *172*, 567−570.
(47) Fleet, M. E. Distortion parameters for coordination polyhedra. *Mineral. Mag.* **1976**, *40*, 531−533.
(48) Dikhtiarenko, A.; Villanueva-Delgado, P.; Valiente, R.; García, J.; Gimeno, J. Tris(bipyridine)Metal(II)-Templated Assemblies of 3D Alkali-Ruthenium Oxalate Coordination Frameworks: Crystal Structures, Characterization and Photocatalytic Activity in Water Reduction. *Polymers* **2016**, *8*, 48.
(49) Keene, F. R.; Ridd, M. J.; Snow, M. R. Investigations of the nature of dehydrogenation of the.alpha.-carbon atom in the oxidation of amines coordinated to ruthenium. *J. Am. Chem. Soc.* **1983**, *105*, 7075−7081.
(50) Yamaguchi, M.; Machiguchi, K.; Mori, T.; Kikuchi, K.; Ikemoto, I.; Yamagishi, T. Facile Dehydrogenation of α-Amino Acids Chelated to a Ruthenium(II) Ion: (α-Imino acidato)ruthenium(II) Complexes†. *Inorg. Chem.* **1996**, *35*, 143−148.
(51) Tamura, M.; Tsuge, K.; Igashira-Kamiyama, A.; Konno, T. A bis-bipyridine osmium(II) complex with an N,S-chelating 2-aminoethanesulfinate: photoinduced conversion of an amine to an imine donor group by air oxidation. *Chem. Commun.* **2011**, *47*, 12464−12466.
(52) Krumova, K.; Cosa, G. *Singlet Oxygen: Applications in Biosciences and Nanosciences*; The Royal Society of Chemistry, 2016; Vol. *1*, pp 1−21.
(53) Gomez, J.; Garcia-Herbosa, G.; Cuevas, J. V.; Arnaiz, A.; Carbayo, A.; Munoz, A.; Falvello, L.; Fanwick, P. E. Diastereospecific and diastereoselective syntheses of ruthenium(II) complexes using N,N′ bidentate ligands aryl-pyridin-2-ylmethyl-amine ArNH-CH2−2-C5H4N and their oxidation to imine Ligands. *Inorg. Chem.* **2006**, *45*, 2483−2493.
(54) Wachter, E.; Glazer, E. C. Mechanistic Study on the Photochemical "Light Switch" Behavior of [Ru(bpy)2dmdppz]2+. *J. Phys. Chem. A* **2014**, *118*, 10474−10486.
(55) Tachiyashiki, S.; Mizumachi, K. Mechanisms of the photosubstitution of ruthenium(II) polypyridine complexes - formation of an intermediate with a monodentate polypyridine ligand and its reactions. *Coord. Chem. Rev.* **1994**, *132*, 113−120.
(56) Knoll, J. D.; Albani, B. A.; Durr, C. B.; Turro, C. Unusually Efficient Pyridine Photodissociation from Ru(II) Complexes with Sterically Bulky Bidentate Ancillary Ligands. *J. Phys. Chem. A* **2014**, *118*, 10603−10610.
(57) Collin, J. P.; Sauvage, J. P. Synthesis and study of mononuclear ruthenium(II) complexes of sterically hindering diimine chelates - implications for the catalytic oxidation of water to molecular oxygen. *Inorg. Chem.* **1986**, *25*, 135−141.
(58) Krężel, A.; Bal, W. A formula for correlating pKa values determined in D2O and H2O. *J. Inorg. Biochem.* **2004**, *98*, 161−166.
(59) Snellenburg, J. J.; Laptenok, S. P.; Seger, R.; Mullen, K. M.; van Stokkum, I. H. M. Glotaran: A Java-Based Graphical User Interface for the R Package TIMP. *J. Stat. Software* **2012**, *49*, 1−22.

DOI: 10.1021/acs.inorgchem.6b02794
Inorg. Chem. 2017, 56, 4818−4828